JOINT DEMAND IN SLAB BEAM BRIDGES

Francisco D. Chitty, MS, Dept. of Civil and Environmental Engineering, Florida International University, Miami, FL

Christina J. Freeman, PE, Florida Department of Transportation, Tallahassee, FL

David B. Garber, PhD, PE, Dept. of Civil and Environmental Engineering, Florida International University, Miami, FL

ABSTRACT

Slab beam superstructure systems are novel solutions currently implemented in short-span bridge applications (less than 65 feet) by different US Departments of Transportation. The Florida Department of Transportation (FDOT) developed one such system (Florida Slab Beam) that specifies adjacent, precast, prestressed slab beams with a cast-in-place (CIP) deck and joint cast all together to act in composite action during service loads. A prototype joint geometry has been developed to expedite the superstructure construction process by eliminating the use of a CIP deck and implementing ultra-high-performance concrete (UHPC) as joint material. This presentation will describe flexure testing of the developed joints and numerical analyses performed to study the full-scale strength and fatigue performance of the longitudinal connection in multi-beam systems with a 30-foot length. Numerical analyses were used to determine the service-level and ultimate strength-level stresses experienced in the joint for different beam configurations and loading schemes. The presentation will also include a discussion on the load transfer mechanisms and moment distribution factors. Results from these analyses were used to plan similar laboratory testing of the full-scale beams.

Keywords: Accelerated Bridge Construction, Slab Beam Bridges.

INTRODUCTION

Slab beam systems have been used in short-span bridge construction in the United States since the beginning of prestressing. Different cross-section geometry iterations have been produced by many departments of transportation, but the construction principle is the same: the beams are shallow precast, prestressed concrete beams that are placed immediately adjacent to each other jointed together by a longitudinal joint cast with the top deck simultaneously. This construction process ensures that the deck-joint and beam systems behave in composite action ensuring diaphragm behavior. There are also some variations of slab beam systems without a cast-in-place (CIP) deck, requiring transverse post-tensioning or a higher strength joint material.

The Florida Department of Transportation (FDOT) has used slab-beam superstructure systems since the early 1950s.[1] Different iterations of shallow beam systems were used in the past, including: (1) prestressed rectangular slab units with a 10-inch regular concrete closure pour and no topping, (2) prestressed keyed slab units with transverse tie bars in sleeves and a 4-inch CIP reinforced concrete, (3) voided slab units with hollow concrete cores and transverse tie bars in sleeves, and (4) prestressed slab units with grouted shear keys and 6-inch CIP reinforced concrete topping. The current iteration developed by the FDOT engineers[2] is the Florida Slab Beam (FSB). This section is used for short-span bridges (less than about 65 feet) and consists of a shallow precast, prestressed concrete inverted-tee beam with transverse protruding rebars from the web that interlock with the joint and deck reinforcement.

A modified FSB section is currently being developed to accelerate the construction process and decrease the construction time. The alternate FSB geometry is designed to not include a CIP deck, leaving only the longitudinal joint cast with a high-performance concrete as the only mean of jointing mechanism. Small-scale joint testing was initially used to develop a proposed joint detail.[3,4] This joint detail was used in numerical simulations to determine proposed multi-beam full-scale testing of the developed cross section.

PREVIOUS SMALL-SCALE JOINT DEVELOPMENT

Analytical and experimental tests were performed on four different small-scale beam cross sections with four different joint designs by assessing their transverse flexural strength under static and fatigue loading as described by Chitty et al. [3,4]. One joint detail was selected based on the results of the strength and fatigue testing, shown in Fig. 1. The selected joint geometry consisted of a shear key detail with a larger embedment length of the joint reinforcement and geometry to minimize stress concentrations. This cross section was the best performer based on ultimate transverse strength and ductility, performance under cyclic loading, and constructability. The joint characteristics such as: rebar position, embedment length, non-contact lap splice length, and inner precast surface finish were developed following Federal Highway Administration (FHWA) guidelines[5] on joint design and accelerated construction recommendations using ultra-high performance concrete (UHPC).

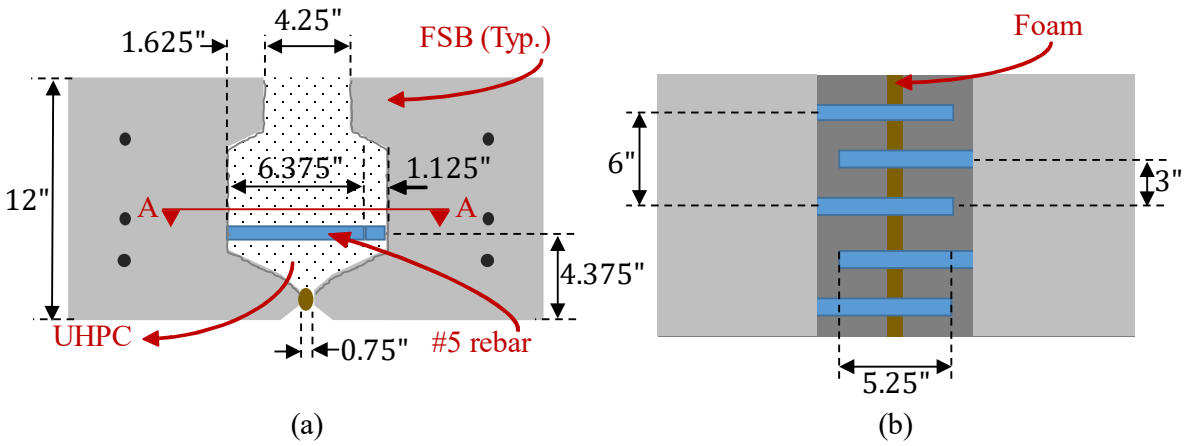

Fig. 1 Modified FSB joint geometry: (a) joint cross section and (b) section A-A

The other reinforcement details for the slab beam section were similar to the original FSB design[2] in terms of rebar distribution, spaces, and sizes. However, the shear reinforcement detail was modified to have four legs across the width of the section without any reinforcement extending out of the top of the section, which was previously required for composite action with the CIP deck. The joint straight transverse rebar protruding from each side are located 4.375 in. from the bottom of the section. This ensured the maximum flexural capacity in the transverse direction while enhancing the ductility strength of the section. The precast joint surfaces were treated with a paste retarder during casting such that an exposed aggregate finish could be achieved following FHWA guidelines[5,6] as follow:

1. Select a commercially available paste retarder agent that ensures an exposed aggregate surface finish to at least ¼-inch amplitude.
2. The set retarding agent is required to be painted on the joint side forms 24 hours prior concrete cast.
3. A polyurethane clear coat must be applied on forms if using wood forms prior to the set retarding agent application. This action is performed to avoid early agent activation due to humidity present in wood pores.
4. After casting, joint forms should be removed and the concrete surface pressure washed within 24 hours.
5. Water pressure and distance from joint should be controlled to remove paste without fracturing exposed aggregates.

A proper finish to the precast section ensures good bond between the precast section and UHPC, as shown in Fig. 2.

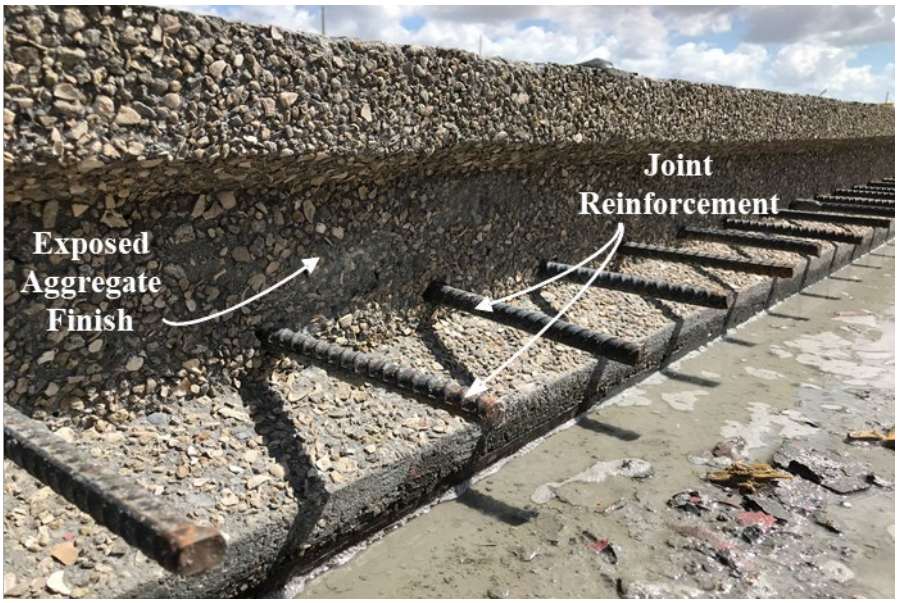

Fig. 2 Joint surface finish after pressure wash

TEST CONFIGURATION

The base case for evaluation of the proposed system is a six-beam, simply-supported bridge with two lanes and 30-foot beam length, which is a typical configuration for many slab beam systems. The 30-foot length was the maximum span length that can be tested experimentally within the lab constraints. The barriers and wearing surface weights were not considered in this preliminary study. The dimensions of the beams in the proposed system are 12 inches deep by 48 inches wide. These are the smallest section dimensions of the current FSB detail. The section dimensions were selected based on the span 30-foot length and the ability to test 2-beam and 4-beam configurations in the available testing frame.

Numerical models were developed for the full six-beam bridge configuration and two-beam configuration. Results from the six-beam analyses were used to evaluate the appropriateness of different two beam configurations. Results from both were used to evaluate the stress transfer through the joints between the beams and possible development of tensile stress in the top of the system.

SIX-BEAM CONFIGURATION

A typical full-width bridge with two lanes and six modified FSBs was used to design the beams for construction and test assessment. The design included the strands and prestressing forces, shear reinforcement, transverse rebar joint reinforcement, and transverse top and bottom ledge reinforcement obtained from the small-scale joint development. A numerical model of the bridge with the designed concrete and steel properties was created to investigate the stresses in the beams and joints that would be expected when a truck load is applied in different locations across the width of the bridge at midspan. A full axle of an AASHTO[7] HL93 truck

was applied at three different positions across the width of the six-beam system at midspan, as shown in Fig. 3: (a) mid-width, (b) off-center, and (c) outside of an outside lane.

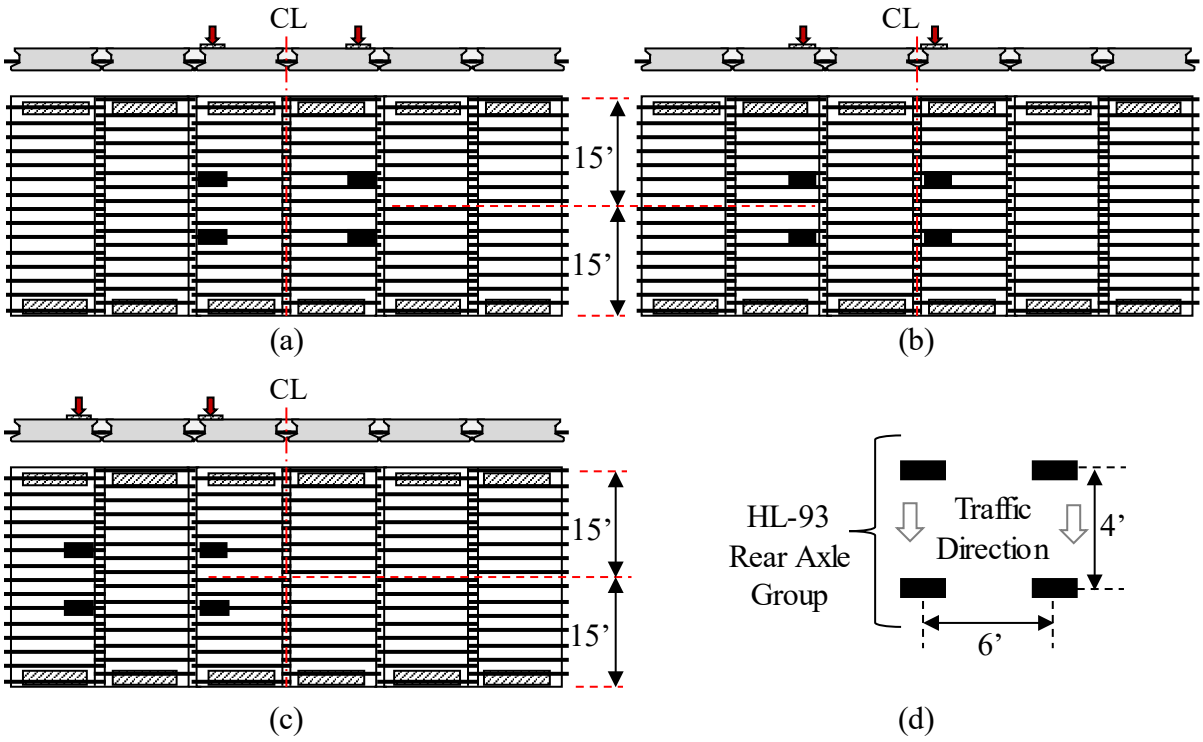

Fig. 3 Midspan load locations (cross-section and plan view) in numerical model: (a) center, (b) off center, (c) outside lane, and (d) HL-93 rear axle group detail

TWO-BEAM CONFIGURATION

A two-beam configuration was used to model the behavior of one joint of the six-beam, simply-supported bridge. Similar to the six-beam configuration, the loading type is based on the AASTHO HL-93 truck loading[7]. The half-axle loading is achieved by applying only one rear, half-axle at the center of the span immediately adjacent to the joint. This loading scheme is similar to a four-point bending test regularly used to assess the flexural behavior and has been used by other researchers[8–10] to assess the performance of multi-beam systems.

Several different two-beam configurations were investigated through numerical analyses. Two loading scheme options were identified as the most critical and practical load applications locations to assess the two-beam system demand, shown in Fig. 4. The two different two-beam load configurations shown, with a full truck axle centered on the two-beam system (Fig. 4 (a)) and with a half truck axle off center on the two-beam system (Fig. 4 (b)), could represent any two beams of the six-beam system. An example of the relationship between the two-beam and six-beam systems is highlighted in Fig. 4.

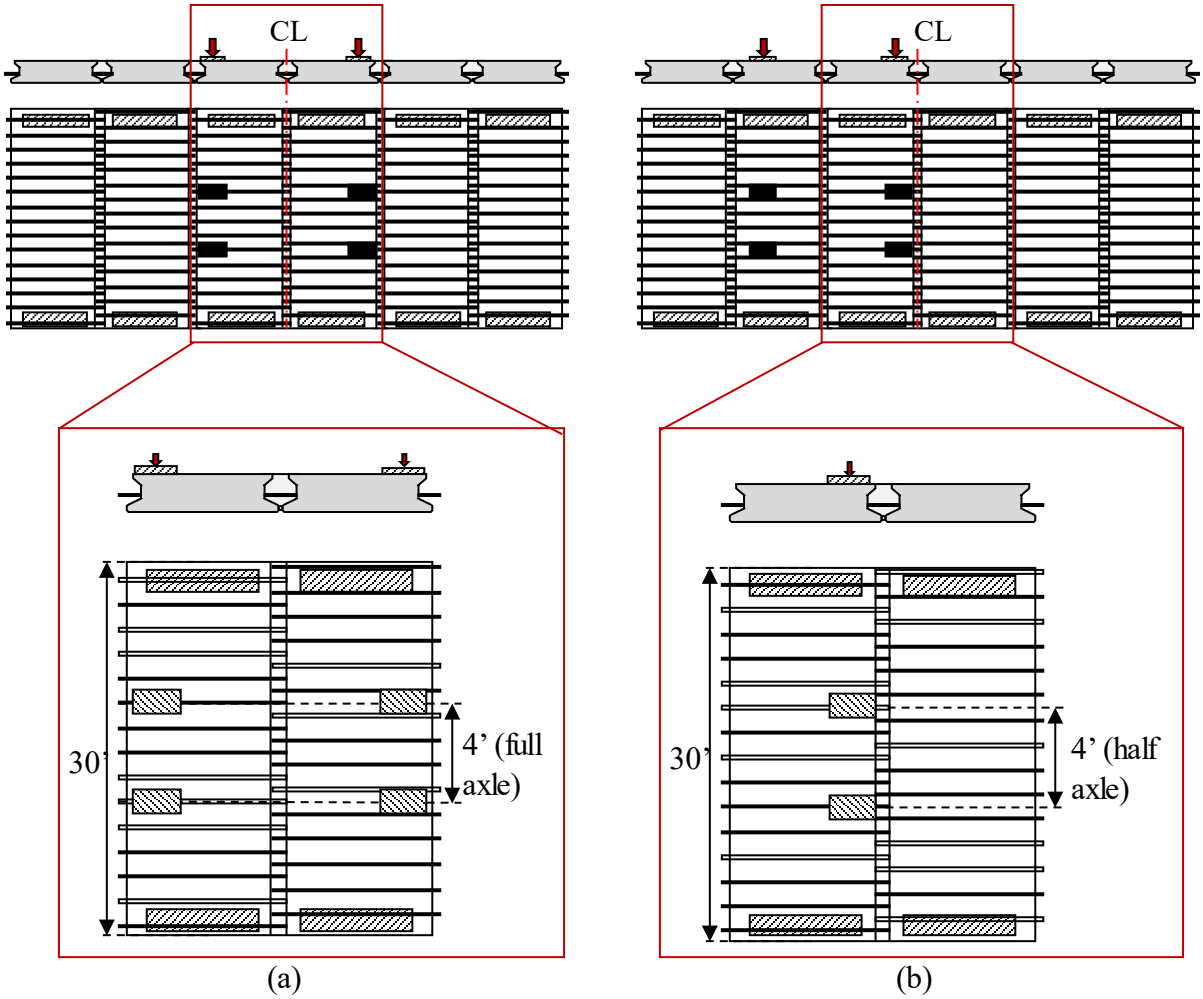

Fig. 4 Midspan load locations (cross-section and plan view) in numerical model related between six-beam and two beam models: (a) center and (b) off center

TWO-BEAM CONFIGURATION: TEST SETUP

The two-beam configuration will be tested using the loading cases shown in Fig. 4. The test setup that will be used to test the two-beam system is shown in Fig. 5. Similar boundary conditions and load were used in the numerical analyses.

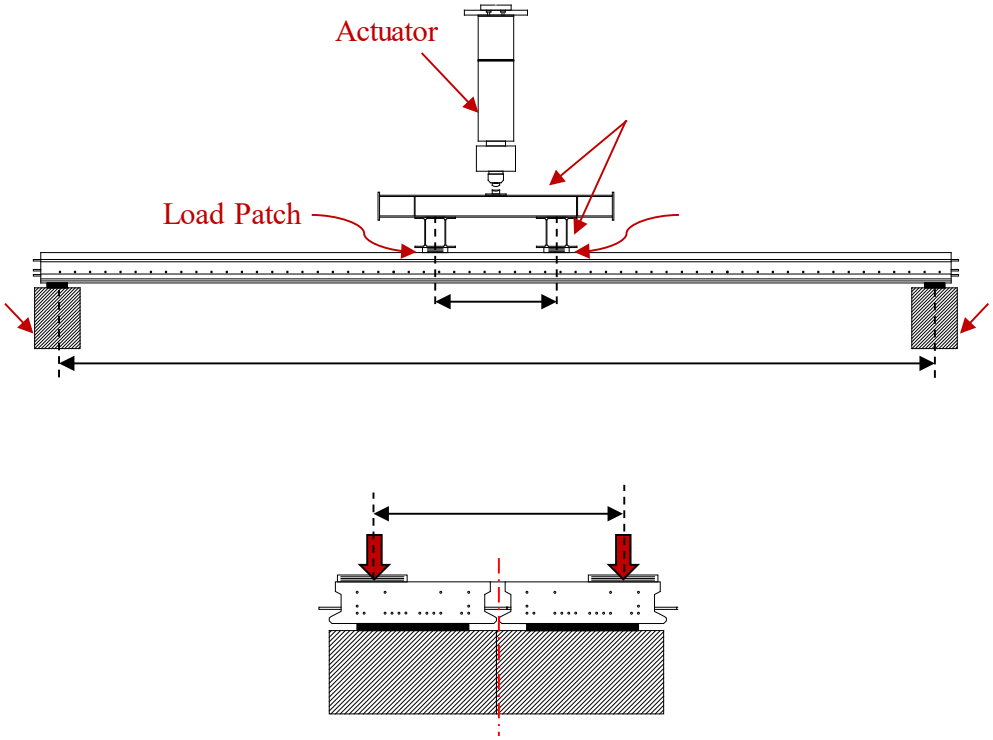

Fig. 5 Test setup for one loading case for two-beam configuration (a) elevation and (b) section views

NUMERICAL MODELING ASSUMPTIONS

Numerical models were developed in ATENA®: a commercial non-linear finite element analysis software for modeling reinforced concrete elements including concrete crushing and reinforcement yielding[11]. Models that were initially developed for the small-scale joint tests were validated through the small-scale experimental program and expanded for the full-scale testing. Numerical models were developed for the six-beam and two-beam systems described above.

MATERIALS DEFINITION

Several assumptions were made to define the model properties as there were not preliminary materials analyses, and they are listed as follow:

1. *Meshing*: A 4-inch mesh size with tetrahedra elements was used for all models.
2. *Precast Concrete*: The precast beam concrete was modeled using the recommended reinforced conventional concrete model[11] (CC3DNonLinCementitious2).
3. *Reinforcement*: The shear stirrups were modeled using a simplified approach by modeling the concrete as a volume material and stirrups as smeared reinforcement with reinforcement ratio depending on the steel direction. Only the transverse steel (#5 rebar), protruding from the precast element to the joint, and the strands (0.6-in

diameter) were modeled as 1D reinforcement for better analysis efficiency of large models.

4. *Strand Design*: The strand layout was determined through conventional design of a two-lane, 30-foot bridge with 12-inch deep slab beams. Three strand layers were used: four top strands to control release and camber, two middle strands at the outermost positions on each side, and 12 strands at the bottom. The top strands were prestressed up to 10 kips per strand, and the middle and bottom strand layers up to 43.9 kips per strand, for a total prestressing force of 615.16 kips
5. *UHPC*: The UHPC material was modeled with the same concrete model as the precast element, but with a larger fracture energy, tensile strength, and stiffness based on a steel fiber content of 2-percent by volume. The fracture energy was deterministic in the UHPC material assumption as there was no simplified approach to model the smeared fiber reinforcement[12]. This assumption showed good correlation when the small-scale model specimens of joints were compared to the actual experimental behavior from previous testing[3,4].
6. *Joint Interface*: The interface between precast concrete and UHPC was assumed to be a perfect bond. This was chosen because previous researchers[5] have found good precast-to-UHPC bond when the joint was designed with the proper aggregate exposure finish

The reinforced concrete and steel materials used in the model definition are shown in Table 1.

Table 1: Concrete and steel material definitions

Section	Compressive Strength (f'_c)	Tensile Strength (f'_t)	Yield Strength (f_y)	Young's Modulus (E_c)	Fracture Energy (G_f)
Beam	10.3 ksi	0.46 ksi	--	5,788 ksi	0.457 lb/in
Joint	20.0 ksi	1.2 ksi	--	7,200 ksi	0.589 lb/in
Joint Steel	--	--	60 ksi	29,000 ksi	--
Strands	--	--	243 ksi	29,000 ksi	--

The regular rebar response was defined with a bilinear stress-strain function with an assumed ultimate stress of 96.6 ksi as used in the small-scale beam steel properties. The strands response was defined with a tri-linear function to such that the prestressing stage and loading stage could be modeled. The strands prestressing stress was 204.4 ksi and ultimate stress was defined as 270 ksi.

MODEL DEFINITION

A simply-supported test setup was used for all beam configurations. Because the model is symmetric in the longitudinal direction, the full beams were modeled as half beams to decrease computational analysis demand, as shown in Fig. 6. The models consisted of a roller support under one bearing end and vertical roller with the rotation restrained at the center. The principal axes are longitudinal (Z-Z blue axis), transverse (X-X red axis), and vertical (Y-Y green axis)

described for all the models. The stress sign convention is positive for tension and negative for compression.

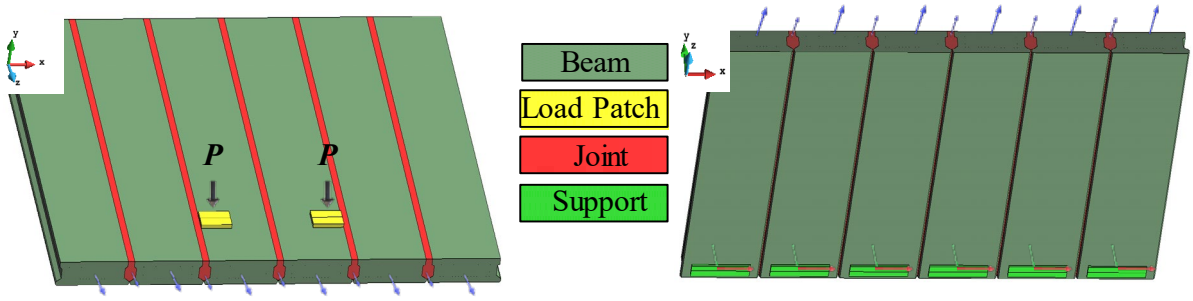

(a) (b)

Fig. 6 Model Definitions: (a) top view for center load condition and (b) bottom view for center load condition (similar to others)

Construction and load stages were used in the system modeling to account for the prestressing, self-weight, and loading to failure. The following stages were defined for the analyses:

1. *Prestressing and self-weight*: A preliminary prestressing stage was defined with at least 10 load steps to create the expected system camber. An initial locked-in strain was defined for each of the strands based on the specified prestressing (after elastic shortening losses). The self-weight of the system was also applied incrementally during each load step. The joint material was defined with no stiffness or strength during this stage.
2. *Casting of UHPC joints*: After the prestressing stage was completed, the UHPC weight application was modeled using 10 more steps.
3. *Loading to failure*: The UHPC was assigned its expected strength and stiffness for this stage. Load was then applied to each patch incrementally at 2 kips per step until the failure of the system occurred.

This procedure was used for all numerical analyses. Both force-controlled and deflection-controlled analyses were used for the analyses. Force-controlled analyses were used when the load was not centered on the width of the bridge. Deflection-controlled analyses were used when the load was applied at mid-width of the bridge.

NUMERICAL RESULTS

A sample of the results from numerical analyses of the six-beam and two-beam configurations are presented in this section.

SIX-BEAM CONFIGURATION

The longitudinal (Z-Z) and transverse (X-X) stress maps when 94 kips per load point are applied to the system for the three load cases for the six-beam configuration are shown in Fig. 7. The load value of 94 kips was selected as it is immediately after the system begins to exhibit

a non-linear respond for all three cases. Tension and cracking developed on the bottom of the six-beam system for all three load cases near the loading points. Small transverse tensile stress and minor transverse cracking were only observed on the top opposite side of the system (marked in yellow) when the off-center region and outside lane were loaded, shown in Fig. 7 (d) and (f), respectively.

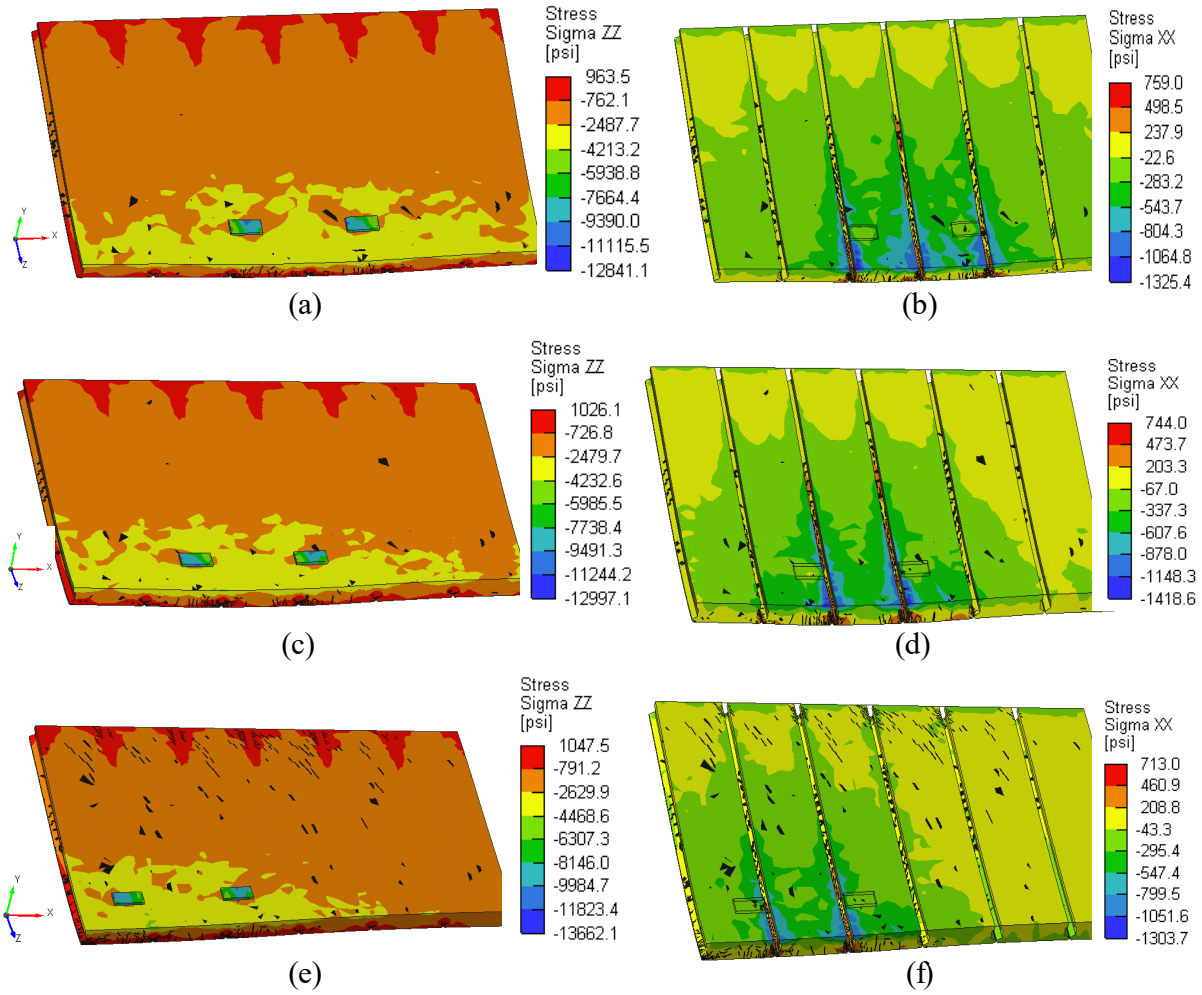

Fig. 7 Stress maps for three load cases for the six-beam configuration: (a) longitudinal and (b) transverse stresses when center loaded, (c) longitudinal and (d) transverse stresses for off-centered loading, and (e) longitudinal and (f) transverse stresses for exterior lane loading

SIX-BEAM CONFIGURATION: DISTRIBUTION FACTORS

The distribution factors were also calculated for the six-beam configuration based on numerical analyses. AASTHO LRFD[7] recommends moment and shear distribution factors based on the superstructure type, girder materials, location of loads, number of loaded lanes, among other characteristics; however, the objective of the study is to determine numerically and experimentally how the load is carried from one beam to another while moving the load axle transversely in the span center. The bottom longitudinal strain of each beam can be measured

to obtain the ratio of strain in a single girder to the summation of strains in all the girders as shown in Equation (1). This method is typically used to determine girder distribution factors based on experimental testing.[13–16]

$$GDF_i = \frac{M_i}{\sum_{j=1}^{k} M_j} = \frac{ES_i\varepsilon_i}{\sum_{j=1}^{k} ES_j\varepsilon_j} = \frac{\frac{S_i}{S_l}\varepsilon_i}{\sum_{j=1}^{k} \frac{S_j}{S_l}\varepsilon_j} = \frac{\varepsilon_i\omega_i}{\sum_{j=1}^{k} \varepsilon_j\omega_j} \quad (1)$$

where:

M_i = bending moment at the i-th girder
E = modulus of elasticity
S_i = section modulus of the i-th girder
S_l = typical interior section modulus
ε_j = maximum bottom-flange static strain at the i-th girder
ω_i = ratio of the section modulus of the i-th girder to that of a typical interior girder

Equation (1) can be further simplified if all the girders have the same section modulus (ω_i = 1.0) to Equation (2).

$$GDF_i = \frac{\varepsilon_i}{\sum \varepsilon_i} \quad (2)$$

Numerical models were developed for the six-beam configuration with a half-axle truck load centered on each of the beams. The transverse stresses in the beams for loading of three of them with an approximate 92-kip load is shown in Fig. 8. Some transverse tension developed in the top of the system away from the loads when the outside two beams were loaded. Transverse tension developed on the bottom of the beams under the load point.

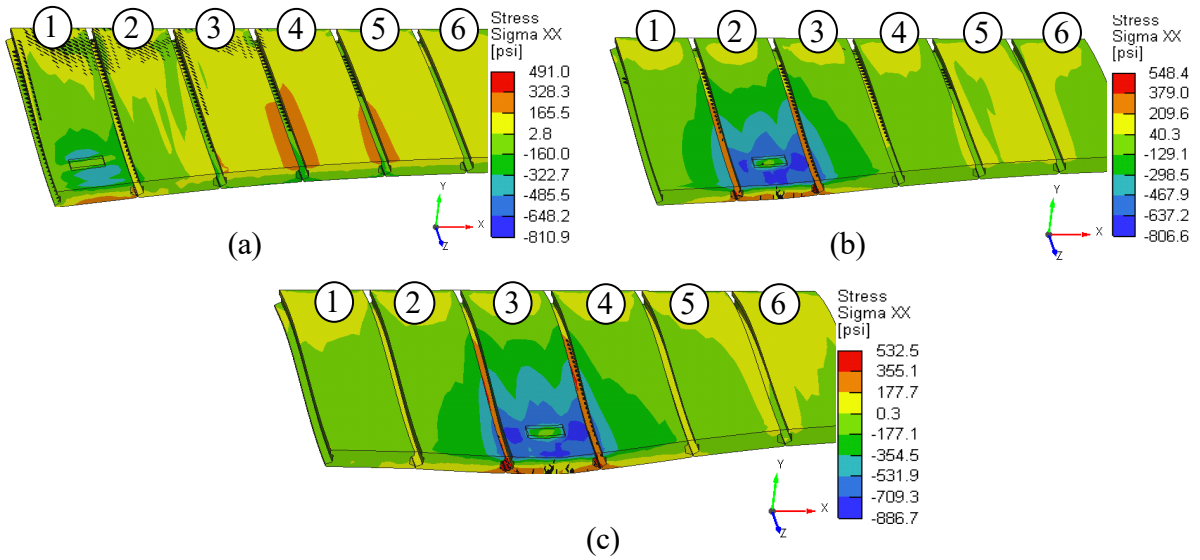

Fig. 8 Transverse stresses with single point load centered on (a) Beam 1, (b) Beam 2, and (c) Beam 3 for distribution factor determination (P = 92 kips)

Longitudinal strain monitors were placed at mid-width underneath each beam. The monitors measured the strain in the system caused by the applied load centered on Beam 1, Beam, 2, and Beam 3, individually. The distribution of moment in the six-beam system were then calculated using Equation (2) and the results plotted as shown in Fig. 9. Only Beam 1, Beam 2, and Beam 3 load cases are shown as they are equivalent to Beam 6, Beam 5, and Beam 4, respectively.

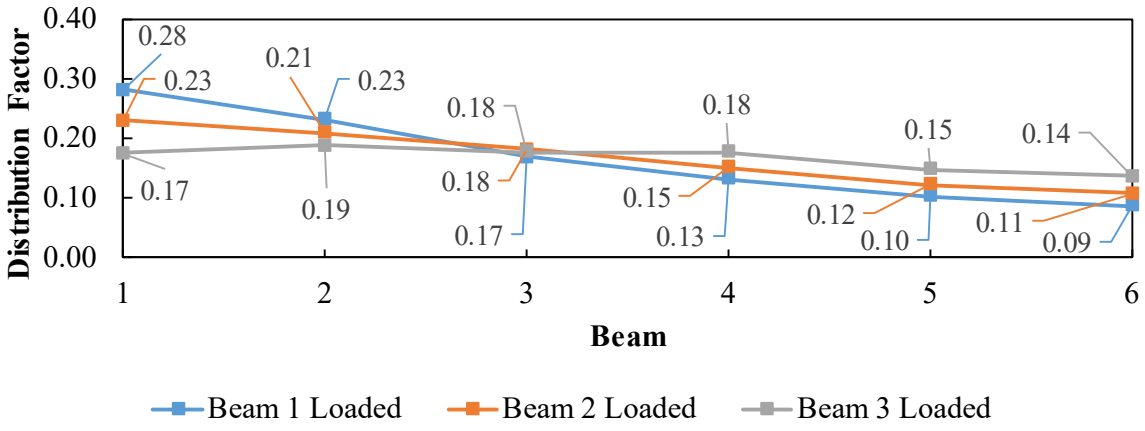

Fig. 9 Distribution Factors found using proportional strain approach

TWO-BEAM CONFIGURATION: LOAD CASE 1

The applied load versus midspan deflection plot for Load Case 1 (full-axle loading) of the two-beam configuration is shown in Fig. 10, and the transverse stresses (in the X axis perpendicular to the joint) are shown Fig. 11. The load versus deflection response remains linear to just above 30 kips per load patch indicating that the system will remain linear well above service loads. Transverse tension was observed on the top of joint for this load case, but stresses were well below the tensile strength of the concrete in the precast section and UHPC in the joint. This would suggest that there would not be any debonding expected along the joint interface. The expected ultimate capacity per patch is 46.4 kips, which is approximately two times the single beam capacity.

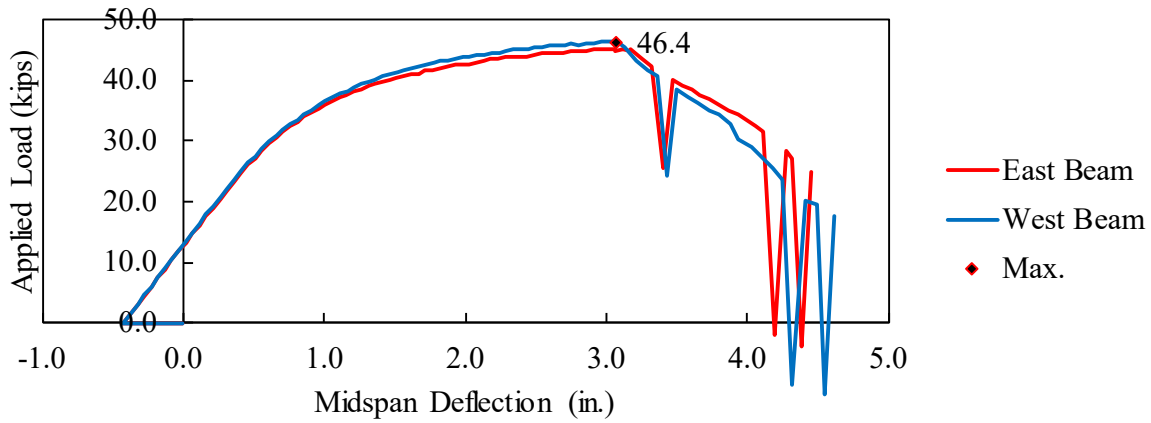

Fig. 10 Estimated full rear-axle loading response for two-beam configuration

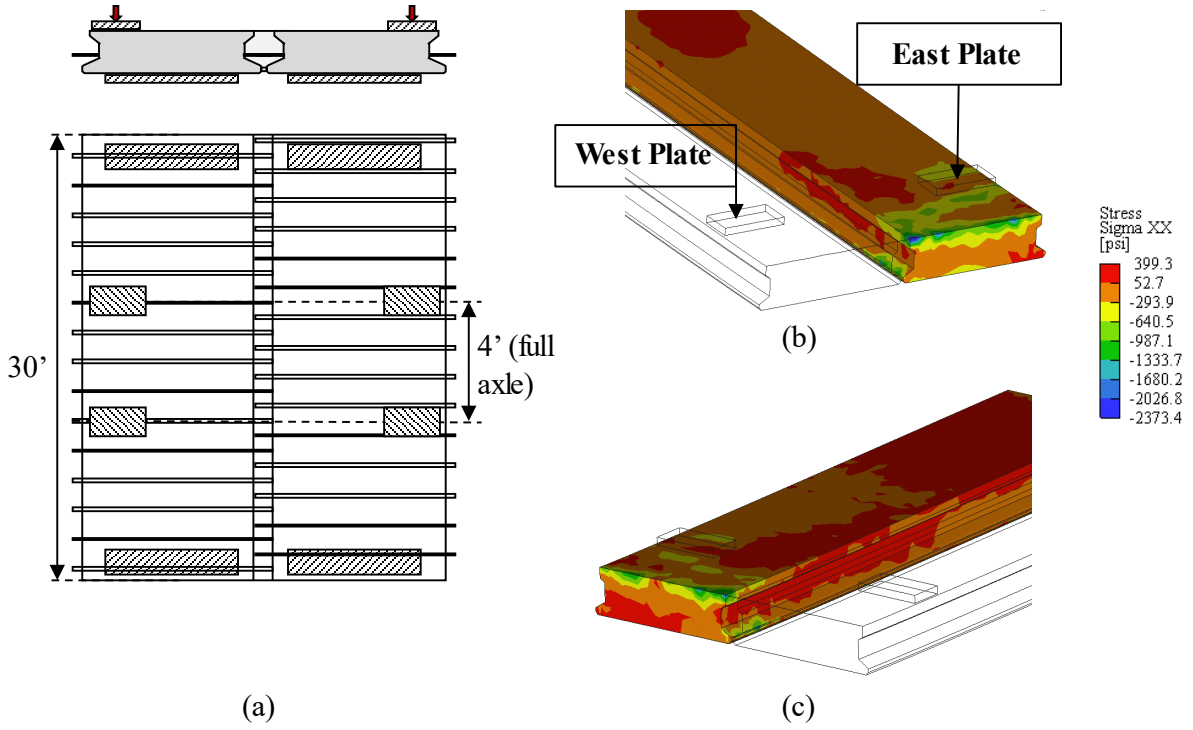

Fig. 11 (a) Full rear-axle specimen testing layout, (b) expected X-X stress pattern at ultimate capacity in East beam, and (c) expected X-X stress pattern at ultimate capacity in West beam

TWO-BEAM CONFIGURATION: LOAD CASE 2

The applied load versus midspan deflection plot for Load Case 2 (half-axle loading next to the joint) of the two-beam configuration is shown in Fig. 12, and the transverse stresses (in the X axis perpendicular to the joint) are shown Fig. 13. The load versus deflection response remains linear to just above 60 kips per load patch indicating that the system will remain linear well above service loads. The expected ultimate capacity reached by both beams is about 92 kips applied to two loading points, which is equivalent to the 46.2 kips applied to four loading points for Load Case 2. The overall behavior of the two-beam configuration under both load cases seems to be similar, suggesting satisfactory performance of the joint to transfer stress from the loaded to the unloaded beam.

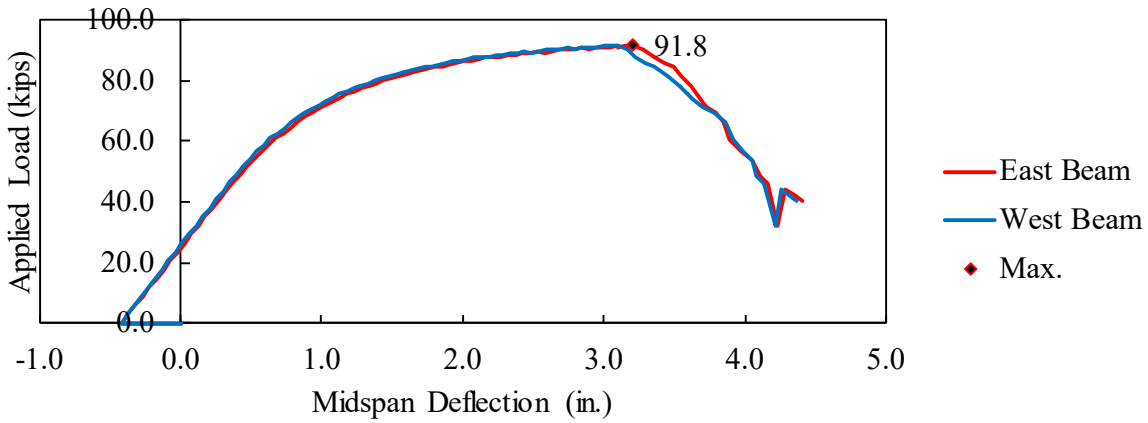

Fig. 12 Estimated half rear-axle loading response for two-beam configuration

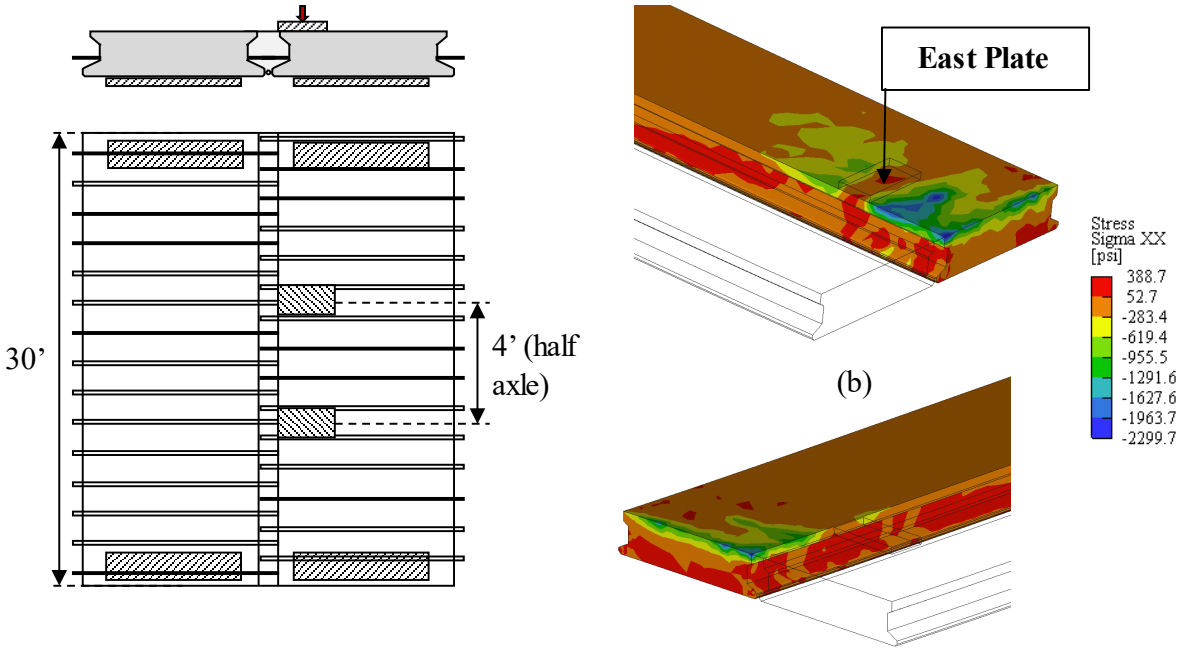

Fig. 13 (a) Half rear-axle specimen testing layout, (b) expected X-X stress pattern at ultimate capacity in East beam, and (c) expected X-X stress pattern at ultimate capacity in West beam

FUTURE EXPERIMENTAL TESTING

Experimental testing is planned for two two-beam configurations and one four-beam configuration. The first two-beam configuration will be tested with Load Case 1 just past the cracking load and Load Case 2 to ultimate load, both static loading. The second two-beam configuration will incorporate fatigue testing with load cases decided on following experimental testing of the first tests. A four-beam configuration will also be tested.

PRELIMINARY CONCLUSIONS AND OBSERVATIONS

A few preliminary conclusions and observations can be made based on the results of the numerical analyses:

- Transverse tension can develop on the top of these systems if exterior beams are loaded at high magnitudes. The magnitude of the transverse tensile stress in the two-beam system appears to be less than the tensile strength of the concrete in the precast section, so debonding at the joint boundary would not be expected. This will be further evaluated through experimental testing to determine if two layers (top and bottom) of reinforcement are required in the joint.
- The largest distribution factor of moment per beam is on the outermost (exterior) beam in the six-beam configuration.
- The full-axle and half-axle loading of the two-beam system are similar with similar deflections in both two-beam systems.
- Typical loading of the six-beam configuration shows the system will respond like a flat-slab system. Some tensile stress can develop and cause cracking on the top of the section if high loads are applied on exterior girders.

Final conclusions and recommendations for cross section design will be made following all experimental testing.

ACKNOWLEDGMENTS

The Florida Department of Transportation financial support and the team of engineers in the structural laboratory is highly acknowledged. The opinions, findings, and conclusions expressed in this publication are those of the author(s) and not necessarily those of the Florida Department of Transportation or the U.S Department of Transportation.

REFERENCES

1. Goldsberry B. Florida Slab Beam (FSB) - Development and Implementation. In Florida Department of Transportation (FDOT); 2015. Available from: http://www.dot.state.fl.us/officeofdesign/Training/DesignExpo/2015/presentations/FSBDevelopmentandImplementation-BenGoldsberry.pdf

2. Florida Department of Transportation (FDOT). Instructions for Developmental Design Standards. Index D20450 Series Florida Slab Beam [Internet]. 2016; Available from: http://www.dot.state.fl.us/rddesign/DS/Dev/IDDS/IDDS-D20450.pdf

3. Chitty F, Freeman C, Garber D. Development of longitudinal joint details for Florida Slab Beam Incorporating Ultra-High-Performance Concrete. In Denver, Colorado: Precast/Prestressed Concrete Institute; 2018. p. 14.

4. Garber D, Chitty F, Freeman C. Development of UHPC Joint Detail for Florida Slab Beam. In: Technical & Scientific Papers. Las Vegas, Nevada; 2018. p. 2.

5. Graybeal B. Design and construction of field-cast UHPC Connections. Federal Highway Administration; 2014 Oct p. 36. (TechNote). Report No.: FHWA-HRT-14-084.

6. Haber Z, De la Varga I, Graybeal B, Nakashoji B, El-Helou R. Properties and Behavior of UHPC-Class Materials. Federal Highway Administration; 2018 Mar p. 153. Report No.: FHWA-HRT-18-036.

7. American Association of State Highway and Transportation Officials (AASHTO). AASHTO LRFD Bridge Design Specification, Customary U.S. Units, 7th Edition. Washington, D. C.; 2014.

8. Yuan J, Graybeal B, Zmetra K. Adjacent Box Beam Connections: Performance and Optimization. Federal Highway Administration; 2018 Feb p. 129. Report No.: FHWA-HRT-17-093.

9. Grace N, Jensen E, Matsagar V, Penjendra P. Performance of an AASTHO Beam Bridge Prestressed with CFRP Tendons. Journal of Bridge Engineering - ASCE. 2013;18:110–21.

10. Grace N, Jensen E, Noamesi DK. Flexural Performance of Carbon Fiber-Reinforced Polymer Prestressed Concrete Side-by-Side Box Beam Bridge. Journal of Composites for Construction - ASCE. 2011;15:663–71.

11. Cervenka V, Jendele L, Cervenka J. ATENA Program Documentation - Theory. Cervenka Consulting; 2016 Dec p. 330.

12. Pryl D, Cervenka J. ATENA Program Documentation - Troubleshooting Manual. Cervenka Consulting; 2018 Oct p. 65.

13. Cai CS. Discussion on AASTHO LRFD Load Distribution Factors for Slab-on-Girder Bridges. Practice Periodical on Structural Design and Construction - ASCE. 2005;10:171–6.

14. Kim S, Nowak AS. Load distribution and impact factors for I-girder bridges. Journal of Bridge Engineering. 1997;2:97–104.

15. Menkulasi F, Roberts Wollmann CL, Cousins T. Live-Load Distribution Factors for Composite Bridges with Precast Inverted T-Beams. Journal of Performance of Constructed Facilities. 2016;04016045.

16. Sennah KM, Kennedy JB. Load Distribution Factors for Composite Multicell Box Girder Bridges. Journal of Bridge Engineering - ASCE. 1999;4:71–9.